Journal of Catalysis 236 (2005) 221-232

Synthesis and functional verification of the unsupported active phase of V_xO_y catalysts for partial oxidation of *n*-butane

M. Hävecker*,[1], N. Pinna[3], K. Weiß[1], H. Sack-Kongehl[1], R.E. Jentoft[1], D. Wang[1], M. Swoboda[1], U. Wild[1], M. Niederberger[2], J. Urban[1], D.S. Su[1], R. Schlögl[1]

[1]Department of Inorganic Chemistry, Fritz-Haber-Institute of the MPG, Faradayweg 4-6, 14195 Berlin, Germany
[2] Max-Planck-Institute of Colloids and Interfaces, Colloid Dep. 14424 Potsdam
[3]Martin-Luther-Universität Halle-Wittenberg, Fachbereich Chemie, Institut für Anorganische Chemie, 06099 Halle (Saale)

* Corresponding author: e-mail mh@fhi-berlin.mpg.de, phone +49 30 8413 4422, fax +49 30 8413 4677

Abstract

We studied unsupported V_xO_y nanoparticles prepared by a novel non-aqueous route in the selective oxidation of *n*-butane to maleic anhydride. The evolution of the electronic and geometric structure of the material was characterized by X-ray photoemission spectroscopy, electron energy-loss spectroscopy, transmission electron microscopy and electron diffraction before and after the reaction at different temperatures. A change from a water mediated C-C bond cracking functionality of the catalyst forming acetic acid to an oxidizing functionality resulting in maleic anhydride was observed. It was found that the particles did undergo a radical modification of the geometric and electronic structure that finally resulted in V_2O_5 crystals. Experimentally derived conclusions will be related to some conceptual claims from the literature.

Keywords: nanostructure, vanadium oxide cluster, micro-reactor, *n*-butane oxidation, structure/activity relationship

1. Introduction

Despite extensive research and contribution to the literature, the understanding of the mode of operation of vanadium based oxidation catalysts is still incomplete [1-4 and references therein]. For the oxidation of *n*-butane to maleic anhydride the technical catalyst is vanadium-phosphorus-oxide (VPO) [5, 6], representing a complex material being composed of a variety of phases [7-9]. Some experimental results suggest that in VPO the structure of the catalytically active species is only weakly related to the average bulk structure [10, 11]. It was suggested that the VPO bulk acts as a support material and reservoir for the constituents of the active structure. Therefore, approaches to establish a structure / activity relationship for VPO that are based on bulk structural data would be at least ambiguous. It seems to be necessary to study model systems with a simplified structure but with relevant catalytic properties.

In contrast to numerous studies of the structure / activity relationship of supported vanadium oxide catalysts [3, 12 and references therein] we investigated unsupported nanocrystals avoiding the complication of support effects. For catalysts containing approximately a monolayer coverage of surface vanadia, the number of converted *n*-butane molecules per vanadium atom was a strong function of the specific oxide support [13]. In our case, the V_xO_y nanoparticles have been synthesized in a controlled way via a simple non-aqueous process involving the reaction of vanadium isopropoxide with benzyl alcohol and subsequent solvothermal treatment [14]. This synthesis approach is widely applicable for the preparation of diverse metal oxide nanopowders with high purity such as $BaTiO_3$ [15, 16], SnO_2, In_2O_3 [17] or HfO_2 [18]. A very small amount of the obtained vanadium oxide powder with a homogeneous, well defined structure and defined morphology has been tested in a microreactor to study the catalytic properties.

This approach to investigate the catalytic function of a single phase vanadium oxide has been taken before and concentrated on V_2O_5 [19, 20]. It was found that sizeable activity was always related with “reduced surfaces” meaning that despite the claimed use of the phase V_2O_5 the active material must have been of another structure. These pioneering studies were, in contrast to their intention, not carried

out with model systems being discriminated from "real" catalysts by their rigorous geometric and electronic structural definition. Thin films of single crystal quality of V_2O_5 became recently available [21 - 23]. Their reactivity even towards chemisorption was found to be negligible as long as their surface was long range ordered. Significant reactivity was detected after partial reduction by ion bombardment or by hydrogen atoms. The same observations hold for V_xO_y clusters deposited on single crystalline oxide supports.

Taking these observations into consideration the hypothesis is put forward that catalytic activity depends on defects in V_xO_y phases. It should then be possible to minimize the energy for the creation of the beneficial defects containing the active sites for catalysis by fabricating nanostructured V_xO_y materials. A lower kinetic hindrance for restructuring into the active, defective form from the long range order of the matrix phase can be expected for nanostructures exposing a sizable fraction of their constituting atoms as surface species and occurring in metastable morphologies and structural variants.

In order to fulfil the requirements of a model system it is essential that a suitable structural definition of such a nanoparticle phase is achieved while its catalytic function is verified. As defects are so relevant it cannot be expected that conventional structural analysis with X-ray diffraction is adequate. The present approach uses the methodology of the TEM as analytical tool for geometric and electronic structure determination. This is adequate for nanostructured and defective materials but requires great care when extrapolated from the local scale of the TEM observation to the integral scale of a catalyst test. Meaningful structure-activity relations can only be expected if the scales of the experiments are brought together as closely as is experimentally possible. Such an attempt that focuses on the real or nanostructure of a functional model oxide is carried out here. This was made possible by the construction of adequate equipment both for the reactor and for the detector used in the catalytic testing. The key idea is to minimize the amount of catalyst for testing in order to approach a situation in which TEM data are representative for the whole catalyst. We use only the amount of material that fits on a standard TEM specimen grid for catalytic testing.

2. Experimental

2.1. Preparation

V_xO_y nanocrystals were synthesised by an alkoxide / benzyl alcohol route [14]. All the synthesis procedures were carried out in a glovebox. Typically, 200 mg of the metal alkoxide vanadium(V) triisopropoxide were added to 20 ml of benzyl alcohol. The reaction mixture was transferred into a Teflon cup of 45 ml inner volume, slid into a steel autoclave and sealed carefully. The autoclave was taken out of the glovebox and heated in a furnace (200 °C for 4 days). The resulting black suspension was centrifuged, the precipitate thoroughly washed with ethanol and dichloro methane and subsequently dried in air at 60 °C.

2.2. Catalytic tests

A reactor similar to the one described in detail in Ref. [24] was used for the catalytic tests of the material. A schematic drawing of the main components is shown as Fig. 1a. In brief, the sample was mounted onto a sapphire sample

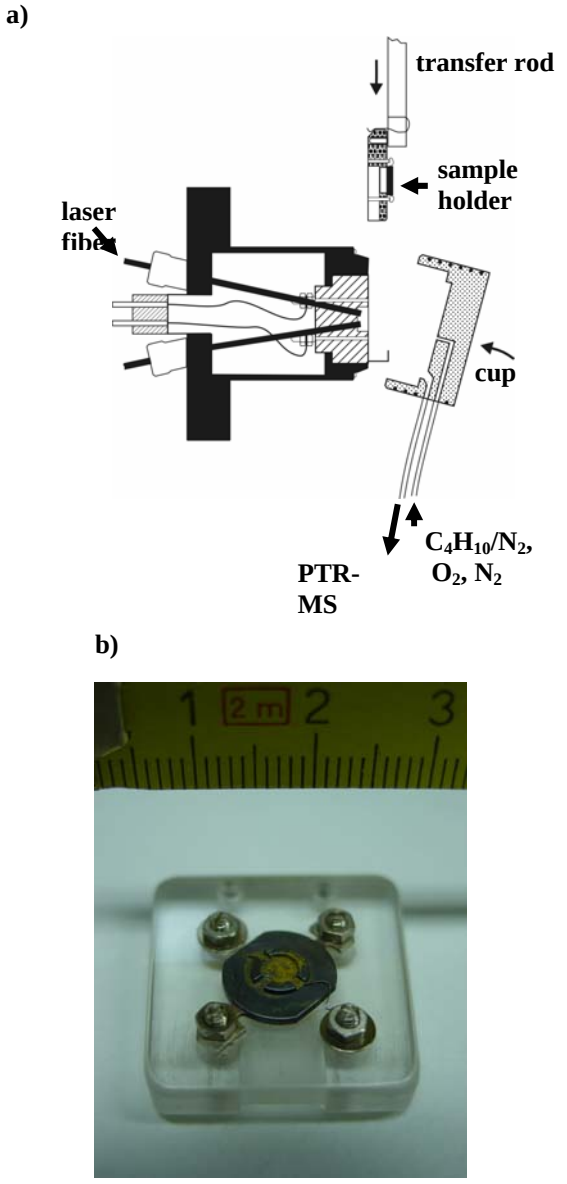

Figure 1: a) Schematic drawing of the reactor. Shown are the main components of the set-up: sample mounted on the sapphire, transfer rod to insert the sapphire into the reactor, movable cup to close the reactor, laser heating from the back. The gas feed is done via mass flow controllers. The reactor outlet is fed into the PTR-MS. **b)** Sample holder used for the experiments. The sample suspension is deposited in the middle of the stainless steel support. This support is mounted onto a sapphire sample holder that is placed inside the reactor after the suspension dried.

holder that is heated from the back by a NIR laser. The reactor has a volume of about 4 ml. It can be opened by a moveable cup and the sample can be transferred out of the reactor without contact to ambient conditions.

For catalytic tests the V_xO_y nanocrystals were first dispersed in ethanol and then one drop of the suspension was released into a ring at the centre of a stainless steel support and dried in air. The ring has an inner diameter equal to the size of a typical TEM grid (around 2 mm). A thermocouple was spot-welded onto this ring for accurate temperature measurement. The stainless steel support was mounted onto a single crystal sapphire sample holder as shown in Fig. 1b. Only a very small amount of catalyst was introduced into the reactor by this method. Thus, the entire amount of catalyst was exposed to identical conditions during the catalytic reaction.

The catalytic characterization was carried out under industrially relevant conditions i.e. oxygen rich conditions at atmospheric pressure. High purity gases were used (butene <1 vpm, butadiene < 0.1 vpm in *n*-butane). A mixture of *n*-butane (1 vol%), oxygen (16 vol%) and nitrogen (83 vol%) was fed into the reactor by calibrated mass flow controllers at a total flow of 22 sccm. The effluent reactor stream was fed in equal shares (each 11 sccm) via heated capillaries into a differentially pumped electron impact mass spectrometer (PRISMA QMS 200, PFEIFFER) and into a proton transfer reaction – mass spectrometer (PTR-MS, IONICON ANALYTIC).

The sensitivity of the electron impact mass spectrometer is approximately 10^{-14} mbar for small molecules like CO_2 as given by the manufacturer and confirmed by our own experience. Due to the differential pumping, this value corresponds to a minimum traceable concentration of 7 ppm - 1 ppm of CO_x in the reactor.

A calibrated version of the PTR-MS (IONICON GmbH, Innsbruck, Austria) equipped with a heated gas inlet capillary system was used. The instrument was operated at a drift tube pressure of 2 mbar. The sample gas was continuously introduced into the chemical ionization cell. Only volatiles that have proton affinities greater than water (proton affinity of H_2O: 166.5 kcal/mol) are ionized by proton transfer from H_3O^+ and subsequently mass analyzed in a quadrupole MS. Sensitivity for oxygenated molecules down to sub-ppb level can be achieved.

The development of selected mass intensities was followed over time (multiple ion detection). The single dwell time for the different masses was adjusted to the concentration. Typically, the accumulation time per point for maleic anhydride (MA) was set to 5 s and it was set to 2 s for all other expected species like acetic acid, crotonaldehyde, 2,5-dihydrofuran and furan. This resulted in an overall time resolution of approximately 4 data points per min if all masses of interest were recorded. Due to the soft energetics of the ionization by proton transfer, mainly nondissociative reactions occur, i.e. a cracking of the target molecule is strongly inhibited. Therefore, it is expected that nearly all intensity is recorded on the parent ion (molecule mass + 1 proton). Thus, no ionization induced fragmentation obscures the link between measured mass spectra and the actual gas composition unlike conventional electron impact mass spectrometry.

As outlined in references [25, 26] a simple relationship exists between the experimentally measured PTR-MS mass spectral intensities (in unit of cps) and the actual absolute concentration in the gas stream. The transmission function of the quadrupole mass filter was taken into account. The temperature of the inlet system and the drift tube was 80 ºC. A rate constant for the proton transfer reaction of $2 \cdot 10^{-9}$ / (cm^3 s) and a residence time of the reactants in the drift tube of 105 µs as given by the manufacturer was assumed.

Although a rather pure primary ion stream of H_3O^+ ions is delivered from the source, we checked for the formation of $(H_2O \cdot H_3O)^+$ clusters (m=37 amu). Cluster formation may become important at high levels of humidity in the inlet gas stream. The formation of these clusters changes the reaction conditions in the drift tube leading to a wrong concentration determination. The proportion of these clusters stayed well below 5% of the H_3O^+ ions under all conditions. Thus, this process was neglected.

2.3. .XPS

Details of the electron spectrometer set-up have been reported earlier [27]. A Leybold LHS 12 MCD instrument was used. The X-ray photoelectron spectroscopy (XPS) measurements have been carried out in the pass energy mode (pass energy: 48 eV). The binding energy (BE) was calibrated to the Au4f (84.0 eV) and $Cu2p_{3/2}$ (932.7 eV) core levels.

2.4. TEM / EELS

For initial transmission electron microscopy (TEM) investigations the catalyst powder was removed from the sample holder with a spatula and placed onto a copper grid covered with a holey carbon film. A design of the sample holder transfer system where the specimen transfer occurs without exposure to air in a glove box is currently being implemented. All measurements were done with a Philips CM200 field-emission TEM equipped with a Gatan energy filter GIF100 for electron energy-loss spectra (EELS) measurements. The microscope was operated at 200 kV. Electron diffraction pattern were taken before the corresponding EEL spectra were recorded.

2.5. TG / DSC - MS

Thermal analysis (combined thermogravimetry (TG) and differential scanning calorimetry (DSC)) was performed with a Netzsch STA 449C Jupiter®. Gas phase products were transferred though a heated silica capillary from the TG/DSC to a Pfeiffer GSD 300 ThermoStar™ mass spectrometer which was run in multiple ion detection (MID)

mode. The sample was heated in 21% oxygen in helium (100 ml/min) at a rate of 5K/min up to 773 K. The sample was eventually held at 773 K for more than 10 hours before it stopped gaining weight. The MS was calibrated for CO_2 using a 0.5 ml pulse of pure CO_2, introduced into the TG in a flow of He at 3 ml/min. The MS was calibrated for water by heating $Cu(SO_4)*5H_2O$ in 100ml/min of 21% oxygen in He at 5K/min to 773 K. The last water peak at between 450 and 550 K, equaling 1 mole water/mole Cu sulfate, was used.

3. Results

3.1. Catalytic Activity

In one type of experiment (Fig. 2a), nanoparticles were heated sequentially from room temperature to 473 K, 573 K, 673 K and cooled down finally to 323 K. In this experiment the absolute amount of products can be compared, because the same particles were used without removing material from the reactor. Afterwards, the reaction was studied in more detail at different temperatures (473 K, 573 K, and 673 K) in single experiments (Fig. 2b – 2d). The material after these treatments was used for the XPS, EELS and TEM studies that are presented in Fig. 4 – Fig. 7. A new drop of the particle / ethanol suspension was used for each temperature step. In these experiments, only the relative amount of products can be compared because it could not be assured that exactly the same amount of material was placed in the active, i.e. hot part of the sample holder in each experiment. The sequential heating experiment shown in Fig. 2a revealed that the onset of the selective *n*-butane oxidation to MA occurred already at temperatures as low as 473 K. Further heating to 573 K caused a strong increase of the MA signal by a factor of 10. The MA signal remained almost constant, when the temperature was increased further to 673 K. The onset of the reaction at relatively low temperature and the weak increase of MA abundance when the temperature is increased from 573 K to 673 K is quite different to the behavior of vanadium phosphorus based catalysts which are the industrially used materials for the selective oxidation of *n*-butane to MA. These catalysts do not show any activity at 473 K and a strong increase in catalytic activity when the reaction temperature is increased from 573 K to 673 K.

The development over time was followed for several masses in detailed scans. The traces for the masses 61 amu, 71 amu, and 99 amu (corresponding to molecule masses 60 amu, 70 amu and 98 amu) are shown for a reaction temperature of 473 K, 573 K and 673 K, respectively, in Fig 2b -2d. The signal on 99 amu can unambiguously be assigned to maleic anhydride. It seems to be reasonable to relate the signal on 61 amu to acetic acid. The 71 amu intensity might be related to crotonaldehyde or dihydrofuran. Crotonaldehyde is sometimes reported in the literature as a by-product of selective C4 olefin oxidation [28]. It is not possible to distinguish isomers with the PTR-MS because the identification of isomers by different fragmentation pattern, as in

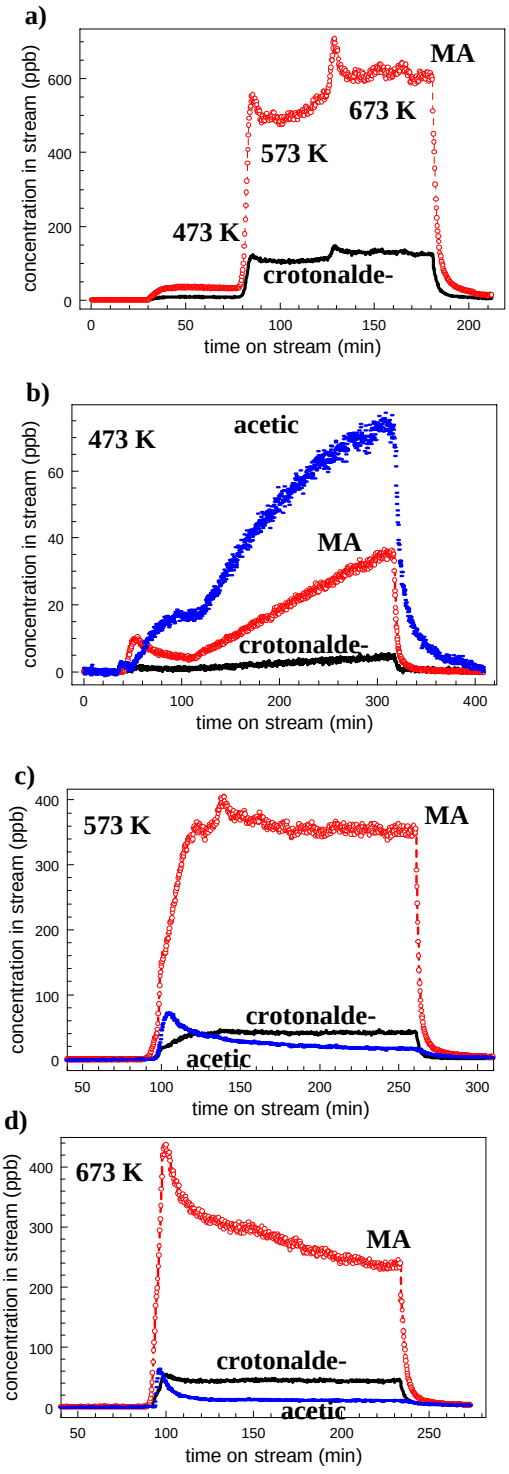

Figure 2: PTR-MS response during the selective oxidation of *n*-butane. **a)** Reaction profile of maleic anhydride (MA) and crotonaldhyde during sequential heating of VO_x nanoparticles to 473 K, 573 K, and 673 K, respectively without taking the material out of the reactor. **b) – d)** Concentration of MA, crotonaldehyde and acetic acid when V_xO_y was heated to 473 K, 573 K, and 673 K, respectively. After each temperature step b) – d) the sample was taken out of the reactor and further characterized as described in the text. A new sample was prepared for each experiment.

conventional electron impact MS, is not possible. Furthermore, traces of furan (molecule mass 68 amu) could be detected at 673 K (not shown).

As mentioned before, the combustion products CO_x and the feed gases C_4H_{10} and O_2 cannot be detected by PTR-MS because these molecules are not protonated by H_3O^+ ions. CO_x could also not be detected by conventional electron impact MS during our experiment, presumably due to low concentration in the product stream. This fact limits the maximum amount of CO_x possibly present during the reaction to 7 ppm – 1 ppm taking the sensitivity of the electron impact MS into consideration (compare to section 2.2). This estimation results in a selectivity of 10% - 40% to oxygenated products. These values compare reasonably well to the selectivities observed for model-supported vanadium oxide catalysts [13]. No conversion of C_4H_{10} and O_2 was detectable by conventional MS, setting the level of reaction to below 1% which is reasonable when taking into account that only a few microgram of catalyst were used. The test can be characterized as ideally differential. Thus, we used the productivity to the oxygenated products acetic acid, crotonaldehyde and maleic anhydride (oxygenate selectivity defined as the product concentration (c_i) ratio: $S_{oxy,i} = \frac{c_i}{\sum_i c_i}$) to get information about the structure / activity relationship for the material.

It can be seen from Fig. 2 that the relative abundances of these products strongly varied in the different temperature regimes. Their quantities are compiled in Table 1. The selectivity S_{oxy} of acetic acid, crotonaldehyde, and MA are shown in Fig. 3. Acetic acid was the dominating species in the gas phase at 473 K (Fig. 2b) with S_{oxy} = 65% (Fig. 3). The signal for this species and for MA increased with time on stream even after 300 min. This is taken as an indication for an incomplete activation of the pre-catalysts similar as it is observed with VPO systems.

Table 1: Concentration of acetic acid (61 amu protonated mass), crotonaldehyde (71 amu) and maleic anhydride (99 amu) derived from data presented in Fig. 2b – 2d.

Temperature	concentration (ppb)		
	61 amu	71 amu	99 amu
200 °C	73,2	4,7	35,6
300 °C	17,6	41,6	354,1
400 °C	10,7	43,9	236,5

MA was the predominant product (354 ppb) when the catalyst material was heated to 573 K (Fig. 2c) with S_{oxy} = 86% (Fig. 3). The signal intensity remained fairly constant over a time span of 120 min indicating structural stability of the catalyst. The concentration of acetic acid (18 ppb, S_{oxy} = 4%) and crotonaldehyde (42 ppb, S_{oxy} = 10%) was much lower than that for MA. The acetic acid signal showed a peak at the very beginning after reaching the reaction temperature of 573 K followed by a steady decrease of the concentration. This is taken as indication for the desorption / diffusion of a limiting constituent for this reaction channel such as OH groups being lost as structural water.

Heating from room temperature to 673 K caused a peak in the MA and acetic acid signal followed by a decrease with time on stream (Fig. 2d). The MA concentration decreased from approximately 400 ppb at the beginning of the heating cycle to 220 ppb after 120 min. The acetic acid and crotonaldehyde concentration was found to be 11 ppb and 44 ppb, respectively. The corresponding selectivity S_{oxy} is 81%, 4% and 15% for MA, acetic acid, and crotonaldehyde, respectively (Fig. 3).

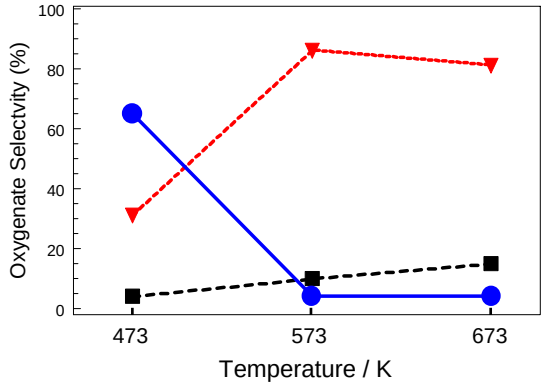

Figure 3: Oxygenate selectivity S_{oxy} for MA (▼), acetic acid (●), and crotonaldehyde (■) at 473K, 573K, and 673K derived from the data depicted in Fig. 2b – 2d.

The reaction tests revealed a pronounced switching of the reactivity between a predominately C-C cleaving and oxidation mode at 473 K to a dehydrogenation and oxidation mode at 573 K and 673 K. Two different catalysts were generated from a common precursor nanostructure by thermal activation in feed. It should be possible to relate this change to structural differences of the two final catalysts. The data further showed that the reactivity at 473 K is related to a slow process increasing the productivity. This points to a slow catalyst transformation and / or to a too low reaction temperature and excludes the notion that the C-C cleaving process is achieved purely through gas phase radical processes. Furthermore, the evolution of the oxygenate selectivity of crotonaldehyde (compared to MA) suggests a different parallel oxidative reaction pathway for this product.

3.2. The Catalyst

3.2.1. Electronic Structure

Electron energy-loss spectra (EELS) probe the bulk electronic structure of individual, microscopically small particles. The shape of the vanadium L-edges and oxygen K-

Table 2: V L_3/L_2 EELS peak ratios for reference compounds with formal V oxidation states varying from +2 throughout +5 and of the catalyst after different thermal treatments in the gas feed.

	reference compounds					catalyst			
	VO	V_2O_3	V_2O_4	V_6O_{13}	V_2O_5	293 K	473 K	573 K	673 K
formal V oxidation state	+2	+3	+4	+4.3	+5				
V L_3 / L_2 peak ratio	1.12	1.21	1.02	0.99	0.96	1.08	1.05	1.00	0.98

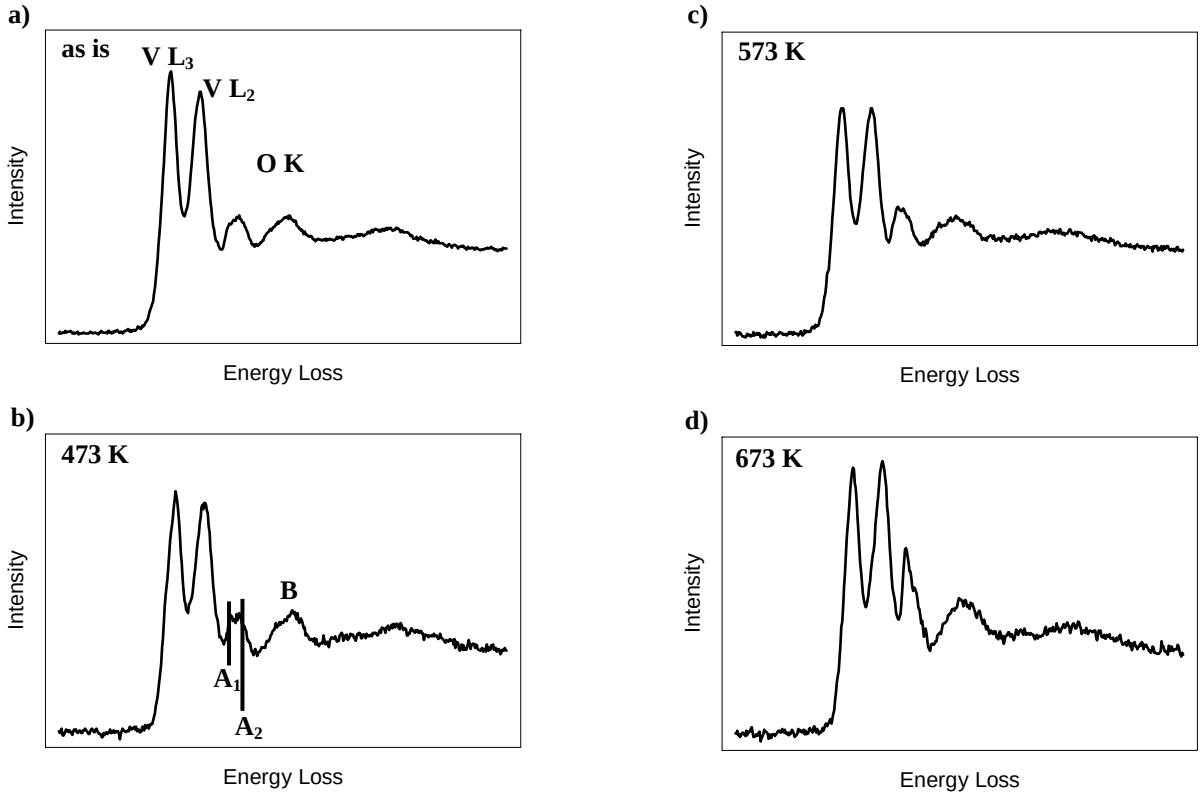

Figure 4: EELS spectra of V_xO_y particles before (a) and after the reaction at 473 K (b), 573 K (c), and 673 K (d), respectively. The spectra can be divided into the V L-edges

edge is strongly related to the oxidation state of the vanadium and to the local geometric structure. As demonstrated in the literature [29, 30] the intensity ratio of the V L_3-edge and the V L_2-edge (corresponding to $V2p_{3/2}$-V3d and $V2p_{1/2}$-V3d, respectively, electronic transitions) is related to the oxidation state of the absorber atom. The V L_2-edge is more intense than the V L_3-edge in V_2O_5, whereas, with decreasing oxidation state, the V L_2 intensity decreases relative to the L_3 spectral weight [31]. The V L_3 / L_2 ratio given as the peak intensity ratio for reference compounds with a formal vanadium oxidation varying from +2 throughout +5 can be found in Table 2. A clear trend becomes visible with the exception of bulk V_2O_3 that exhibits an unexpectedly high L_3 / L_2 ratio. This anomaly of bulk V_2O_3 is probably due to other factors (e.g. hybridization) than the V oxidation state that influences the d-state density and therefore the white line peak ratio. Nevertheless, the V L_3 / V L_2-edge intensity ratio is a fingerprint for assignment of the oxidation state. In the same manner the intensity ratio of the resonances A1, A2 and B at the O K-edge are indicators for the oxidation state of binary vanadia species (compare to Fig. 4b). In general, resonance A1 gains intensity relative to A2 when the material becomes oxidized and the resonances A1 and A2 get more intense compared to resonance B.

Fig. 4 shows the EELS spectra of the as synthesized material (a) and after prolonged treatment in the reaction mixture of *n*-butane and oxygen at 473 K, 573 K and 673 K (b – d), respectively. It can be seen clearly that the V L_3/L_2 intensity ratio decreased when the material was treated at higher temperatures. While the V L_3 white line is more intense for the as synthesized material and after heating in the reaction mixture to 473 K (Fig. 4a and 4b), the white line intensity is equal for the material heated to 573 K (Fig. 4c). Heating to 673 K resulted in a more intense V-L_2 edge than the V L_3-edge (Fig. 4d). The calculated V L_3 / L_2 peak intensity ratio of the V_xO_y particles is summarized in Table 2.

Similar intensity variations could be observed at the oxygen K-edge. The intensity of the resonances A1 and A2 compared to resonance B increased during the treatment. Furthermore, the intensity ratio between A1 and A2 was modified by the treatment in *n*-butane and oxygen. Resonance A1 gained intensity during this process.

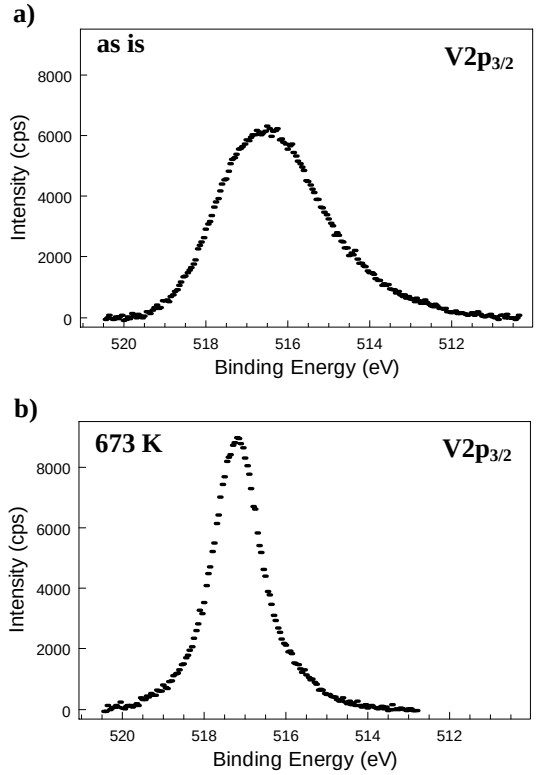

Figure 5: $V2p_{3/2}$ core level XP spectra of the as synthesized V_xO_y nanoparticles (before the reaction) and of the material after the reaction at 673 K.

The surface electronic structure of the material was determined by XPS before the catalytic tests and after the treatment of the nanocrystals at 673 K in the reaction mixture. The macroscopic nature of standard XPS averages over the surface electronic structure of many nano-particles and yields an average information about the oxidation state. The XP vanadium $2p_{3/2}$ core level spectrum of the as prepared material exhibited a broad, asymmetric line shape (Fig. 5a). This indicates a variety of vanadium species of different valences. Taking the known binding energy of binary vanadium oxides into consideration, the as-prepared material consisted of vanadium species with the formal valence of +3 throughout to +5. Details of the composition depend on the assumed line shapes that are not known a priori. After the reaction at 673 K the $V2p_{3/2}$ core level spectrum exhibits a sharp peak with a binding energy of 517.2 eV (Fig. 5b). This is consistent with a formal valence of +5 of the material.

The study of the electronic structure by XPS (averaging, surface sensitive) and EELS (individual particle, bulk sensitive) results in the following conclusion. The as synthesized material holds vanadium particles with a variety of oxidation states. While mainly V^{3+} and V^{4+} were found by EELS, XPS showed some amount of V^{5+} species at the surface, too. In the course of the reaction at different temperatures the particles were oxidized by the feed gas. After prolonged treatment at 673 K almost solely V^{5+} species were found both by EELS and XPS. The oxidation did not occur during sample transfer due to the reaction conditions because for the as-synthesized particles almost no V^{5+} was found. Thus, it was possible to tune the oxidation state of the nanoparticles by the thermal activation in the feed. Except for the final state after heating to 673 K, always a mixture of different vanadium oxidation states was found.

3.2.2- Morphology and geometric structure

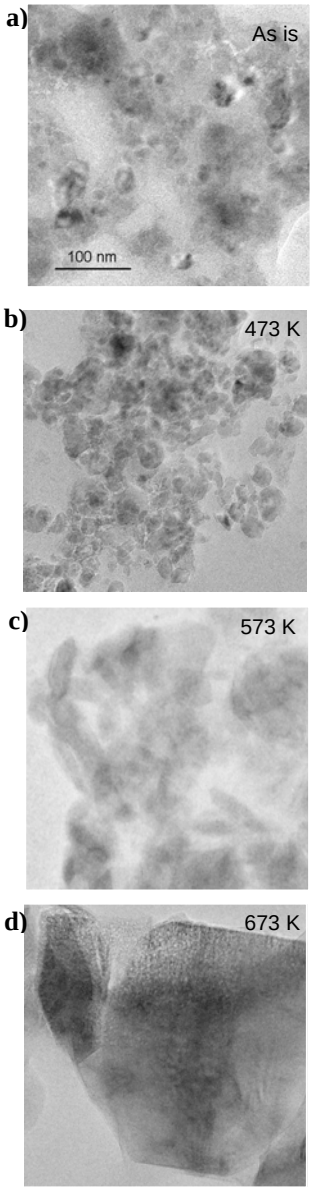

Figure 6: TEM micrographs of the V_xO_y particles before (a) and after the reaction at 473 K (b), 573 K (c), and 673 K (d), respectively.

The oxidation process of the catalyst went along with a strong change of the morphology and the geometric structure. Fig. 6 shows TEM micrographs of the material before (a) and after reaction at 473 K (b), 573 K (c), and 673 K (d), respectively. The material was converted to various small particles after reaction at 473 K indicating the loss of structural water or other volatile species. Re-crystallization started at 573 K. Finally, well developed crystals resulted from the reaction at 673 K.

Table 3: *d*-spacings derived from the electron diffraction pattern of the material before the reaction. The value of 1.94 Å does neither belong to the structure of V_2O_4 nor V_2O_3.

d values measured (Å)	V_2O_4 (tetragonal)		V_2O_3 (rhombohedral)	
	d (Å)	(hkl)	d (Å)	(hkl)
2.69			2.71	(104)
2.44	2.42	(011)	2.48	(110)
2.16	2.14	(111)	2.19	(113)
1.94				
1.82			1.83	(024)
1.68	1.66	(121)	1.70	(116)
1.49			1.47	(214)
1.41			1.43	(300)

The structural dynamics of the material during the reaction was studied by electron diffraction. Characteristic diffraction patterns of the material before (a) and after reaction at 473 K (b), 573 K (c), and 673 K (d), respectively, are shown in Fig. 7. The diffraction patterns of the material before the reaction resulted in a mixture of mainly V_2O_3 and VO_2 crystallites, but there were also other particles present, whose structure could not be identified as standard phases. The analysis of the d-spacings of the material before the reaction is summarized in Tab. 3. The main component of the material after the reaction at 473 K was VO_2, although few crystallites were of an unidentified structure. No V_2O_3 nanocrystals were present after the treatment. After reaction at 573 K, no single vanadium oxide phase could be identified unambiguously from the electron diffraction pattern. The material seems to be a mixture of vanadium oxides but the occurrence of VO_2 crystals can be excluded. The measured *d*-spacings of the material after the treatment at 573 K and their assignments can be found in Tab. 4. The material after the treatment at 673 K consists nearly exclusively of V_2O_5 crystals, exposing their (001) surface to a large extend as basal plane.

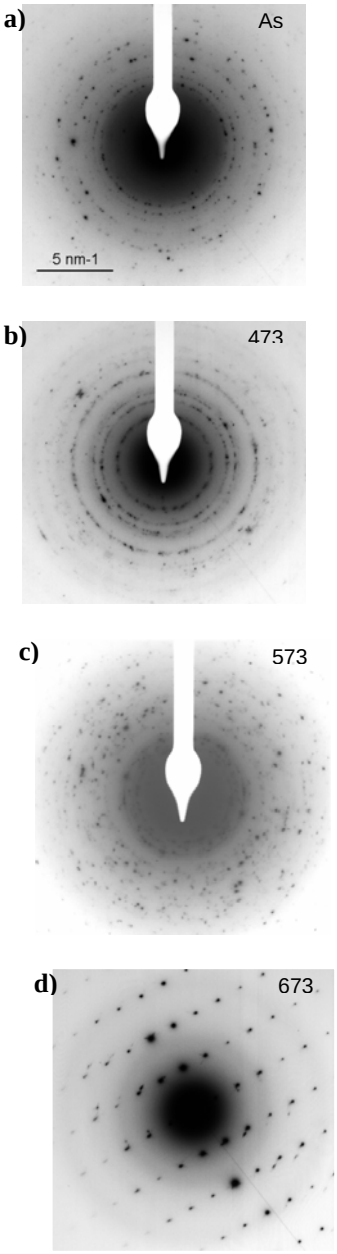

Figure 7: Electron diffraction patterns of the V_xO_y particles before (a) and after the reaction at 473 K (b), 573 K (c), and 673 K (d), respectively.

3.2.3. Release of structural water

The reaction tests revealed a pronounced switching of the reactivity between predominately C-C cleaving and oxidation mode at 473 K to a dehydrogenation and oxidation mode at 573 K and 673 K. To elucidate the role of water release in this thermally activated process, the as synthesized material was characterized using combined thermogravimetric and differential scanning calorimetry with gas phase analysis by mass spectrometry. The result of this TG/DSC-MS measurement in 21% oxygen in He is shown in Fig. 8. The evolution of water (m/z=18) and CO_2 (m/z=44) was observed during the heating of the particles.

Table 4: *d*-spacings derived from the electron diffraction pattern of the material after the reaction at 300 °C. Vanadium oxide phases with similar *d*-spacings are listed for comparison.

d values	V_2O_4 (unknown)	$VO_{1.27}$ (tetragonal)		V_3O_5 (monoclinic)		V_6O_{11} (triclinic)	
measured (Å)	d (Å)	d (Å)	(hkl)	d (Å)	(hkl)	d (Å)	(hkl)
3.38	3.31	3.37	(224)			3.31	(-120)
3.06		3.03	(512)			3.06	(-1-17)
2.62	2.68	2.63	(602)	2.64	(-310)	2.62	(1-24)
2.39	2.43	2.39	(444)	2.42	(-312)	2.42	(016)
2.02	2.03	2.06	(008)	2.00	(022)		
1.77				1.74	(-510)		
1.64	1.65			1.63	(-114)		
1.51				1.51	(-132)		

Water is removed from the sample with three maxima in concentration at 363 K, 513 K, and 573 K. The first maximum in water is the desorption of physisorbed water with no other gas phase products. The next, similarly broad peak in the water concentration with a maximum at 513 K occurred simultaneously with an increase in CO_2 concentration, but the CO_2 evolution had a distinctly different profile (Fig. 8). Thus, we conclude that most of the water production at 513 K results from a different process, i.e. the dehydroxylation of the particles. The final water peak at about 573 K was relatively sharp and occurred with the same profile as the most rapid evolution of CO_2. Furthermore, this process coincided with an exothermal peak in the DSC signal (not shown). This suggests reactions at 573 K that produce both water and CO_2, presumably the combustion of residual CH_x-groups from the preparation procedure.

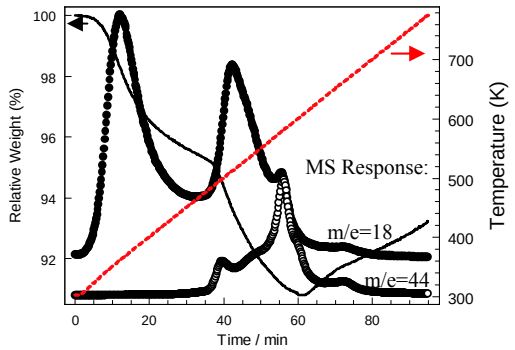

Figure 8: Evolution of the relative weight during heating in 21% oxygen in helium, together with the MS signals for H_2O (m/z=18) and CO_2 (m/e=44).

The TG results show two weight loss steps ending at 483 K and 613 K followed by a weight increase. The first weight loss (about 5%) is ascribed to the desorption of water. Integration of the water signal and application of the calibration factor give a value of 0.936 mg water lost during heating to 473 K. This is in good agreement with the weight loss of 0.90 mg measured by TG. In the second step an additional 4.2% of the initial weight was lost. This weight loss is ascribed to the release of water and the combustion of hydrocarbon residuals as mentioned above. Quantification of the gas phase products allows an estimation of the mass loss due to these products. Based on the scenario that the hydrocarbon residuals have the general formula CH and that water evolving at temperatures above 473 K is from either hydrocarbon combustion or from dehydroxilation, the gas phase products equal 1.92 mg of adsorbed species. However, the weight loss from TG equaled only 1.77 mg. This difference is higher than the expected error for the gas phase quantification (about 4%). In order to close the mass balance another process is required, and this is likely the further oxidation of the vanadium as suggested by the EELS data (Fig. 4b, 4c). Finally, the mass increased with increasing temperature after 613 K (about 2.4% of the initial weight) without further evolution of gas phase products. This mass change is ascribed to the continued oxidation of the particles. After an extended time of heating, this results in V_2O_5 (XRD). This final state can be used as a basis to calculating the vanadium valence at minimum sample mass, and results in a vanadium valance of 4.5 at 613 K, consistent with the results of TEM, EELS and XPS.

The TG-MS experiments allow us to attribute the change in the catalytic reactivity when the particles where heated from 473 K to 573 K (Fig. 3) to loss of OH groups lost as structural water.

4. Discussion

It is quite instructive to compare the catalytic behavior of the V_xO_y nanocrystals described in this report with the information about metal oxide supported vanadia species found in the literature. In the case of supported vanadium oxide catalysts it is reported that the turn over

frequency in *n*-butane oxidation to maleic anhydride declined above a loading exceeding monolayer coverage. It was concluded that this reflects the lower activity of microcrystalline V_2O_5 particles for the oxidation of butane i.e that microcrystalline vanadia was found to be detrimental for the process of maleic anhydride formation. The same mechanism seems to work in the case of unsupported V_xO_y nanocrystals.

Competitive reaction pathways are possible for an adsorbed organic intermediate. The selectivity pattern of the transformation of a specific intermediate depends on several factors, i.e. the intrinsic activity of the active site to which the adspecies is adsorbed, the rates of surface migration or desorption of the adspecies, the reactivity of the adspecies towards gaseous oxygen [32]. These factors are influenced by the specific surface characteristics. Oxygen availability plays a crucial role in the reaction selectivity. If insufficient oxygen is present, then partially oxidized species may desorb from the initial site at the surface of the catalyst. Thus the degree of reduction or the redox ability of the catalyst surface determines the reaction rate and the selectivity to partial oxidation products.

A lowering of the reaction temperature (compared to conventional VPO bulk catalyst for *n*-butane oxidation to MA) was found in the case of supported vanadium oxide catalysts, too. Ruitenbeek et al. and Wachs et al. studied *n*-butane oxidation to maleic anhydride on titania supported VPO catalysts and titania supported V_2O_5 catalyst, respectively [33, 13]. They found that selective oxidation took place at much lower temperature (493 K) than in the case of conventional VPO catalysts. It was concluded that the oxidation of butane to maleic anhydride depends on both the redox properties and the acidic character of the bridging V-O-support bond. This type of bond is missing, of course, for unsupported V_xO_y nanocrystals studied in this report. Ruitenbeek et al. concluded that the activity of titania supported catalysts is related to their reducibility and to the average oxidation state of the vanadium ions on the surface [33].

It is expected that the removal of moisture has a significant influence on the catalytic activity. Surface vanadia species can become hydrated in the presence of moisture. Wachs et al. report a significant coverage of metal oxide supported vanadia species with moisture at temperatures below 473 K (several monolayers) [12, 13, 34]. The dehydration of the vanadia species seems to start at temperatures higher than 473 K. Almost no moisture could be detected with Raman on these metal oxide supported systems at 573 K. The strong activity increase and selectivity change observed in our experiments when the catalyst was heated from 473 K to 573 K coincided with the dehydroxylation of the nanoparticles as revealed by TG-MS.

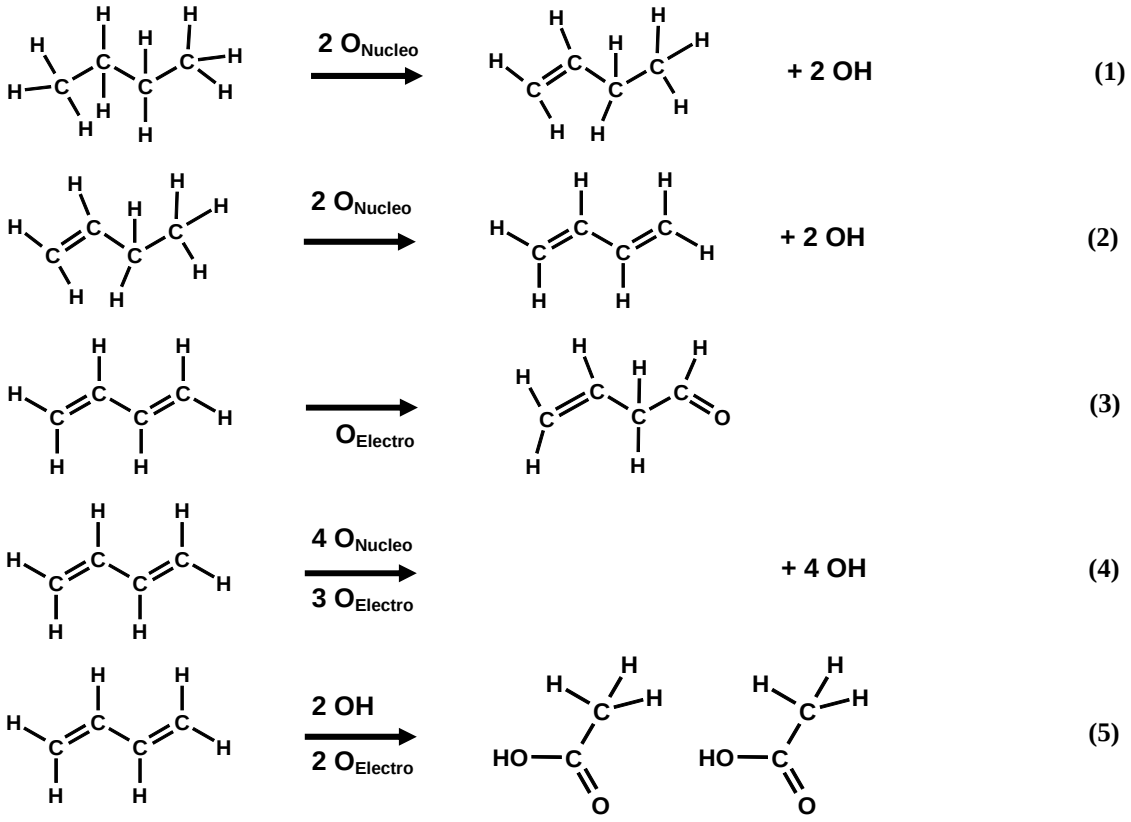

Figure 9: Simplified reaction scheme of the selective oxidation of *n*-butane towards maleic anhydride

The development of the catalytic activity during the isothermal experiments at 473 K and 673 K (Fig. 2b and Fig. 2d) points to an evolution of the catalyst structure, while the steady state behavior at 573 K seems to be the consequence of a mixture of phases. It became evident from XPS and EELS that the electronic structure of the nanoparticles changed from a variety of vanadium species with different oxidation states in the range of V^{3+} to V^{5+} to a material that contains only V^{5+} species (Fig. 4 and Fig. 5). The formation of well-crystallized V_2O_5 is detrimental for the reactivity of the material. This conclusion is supported by the fact, that material that has been heated to 673 K for a prolonged time showed a lower MA yield when it was cooled down to 473 K than a material that was heated from room temperature to 473 K. Defective and nanostructured forms of bulk vanadium oxide seem to be the carrier of the catalytic activity that is absent in V_2O_5 (001) surfaces.

The analysis of the reaction as a function of temperature reveals two different reaction pathways at 473 K and 573 K. We suggest that two different catalyst species are the reason for this observation. Fig. 9 shows a simplified reaction scheme that explains the different functionalities of the catalyst material. At high temperature the catalyst exhibits both a dehydrating and an oxidizing functionality through nucleophilic oxygen O_{Nucleo} and electrophilic oxygen $O_{Electro}$, respectively. This is visualized as reactants O_{Nucleo} and $O_{Electro}$ in the Fig. 9. Additionally, there exist reactive protons (visualized as OH) at low temperature. These reactive protons might be created by the dehydrogenation products. At least the $O_{Electro}$ species must be bound to a reduced metal species. First, butane gets twofold dehydrogenated resulting in an activated butadiene molecule (steps 1 and 2). At low temperature, butadiene might be converted into activated ethylene by C-C bond cracking. Interestingly, ethylene was observed by Chen and Munson as a by-product for *n*-butane oxidation on VPO catalysts [35]. The ethylene molecules add formally water and get oxidized via the aldehyde to acetic acid (step 5). This process might happen either as shown in Fig. 9 or sequentially. This C-C bond cracking functionality is missing at high temperatures and instead the activated butadiene gets oxidized finally resulting in MA (step 4). In an additional, parallel pathway the activated butadiene gets oxidized to but-3-enal (step 3) finally resulting in crotonaldehyde (but-2-enal) via a rearrangement reaction.

From these assumptions about the reaction pathway it can be concluded that at 473 K the catalyst material must contain both V^{5+} sites that can be reduced (reversibly to V^{3+} or V^{4+}) and active OH groups with C-C bond cracking functionality. Candidates for this kind of material are isopolycompounds, i.e. complex hydrate-oxides. Typically, these compounds loose structural water at a temperature around 523 K and as a consequence thereof the water mediated C-C bond cracking functionality is lost, too, and the material forms oxides with a complex structure. The observation of water release in the TG-MS with a concentration maximum at 513 K strikingly supports this conclusion. Around 673 K, thermodynamic stable phases are formed due to the strong self-diffusion of oxygen in these compounds at this temperature. This might be V_2O_5 or V_2O_4 depending on the oxygen partial pressure. Thereby, the catalytic activity gets diminished.

5. Conclusion

The data presented are a strong confirmation of the validity of the approach outlined in the introduction. The application of chemical synthesis procedures from nanotechnology gave access to reproducible precursors for fully functional model oxides of binary unsupported V_xO_y systems. In contrast to model-supported vanadium oxide catalysts, the unsupported model system gave direct excess to structural data of the reactive material. It was possible to follow its structural transformations from a supramolecular system into the highly active selective oxidation phase and into its deactivated stable form of V_2O_5. The present study has produced sufficient amounts of a single phase active material. The amount of material used for catalytic testing was minimized to approach a situation in which the data obtained by TEM are representative for the whole catalyst. Morphological, geometric structural and electronic structural details of the metastable state of V_xO_y were collected which can be used for developing experimentally supported structural models of the active sites. The transient character of those materials being metastable under operation conditions and the strong relevance of the operation conditions on formation and kinetic stability of the material was highlighted.

The simultaneous detection of morphology, geometric structure and electronic structure allows us to draw a series of conclusions for the nature of the active phase. These experimentally derived conclusions substantiate many conceptual claims from the extensive literature and allow to draw a more consistent picture of the function of V_xO_y in partial oxidation. These conclusions cover the following issues:

- *C-C bond cracking versus redox function:* A selectivity change from acetic acid to MA was observed. This finding is ascribed to the change from the water mediated C-C bond cracking functionality forming acetic acid to the oxidising functionality resulting finally in MA as described in Fig. 9.
- *Multiple sites:* A steady formation of crotonaldehyde independent of the main reaction was found (Fig. 3). This implies a parallel process.
- *Relevance of the oxidation state:* Pure V^{5+} is ineffective but maybe only as it exists on defect-free surfaces (vanadyl termination). The co-existence of V^{5+} and V^{4+} as un unavoidable consequence of structural defects is essential for selective oxidation function.
- *Lattice oxygen:* Defect formation is essential. Thus, deep lattice oxygen is an indicator for the defect formation, not a source for selective oxygen (under operation conditions with gas phase oxygen). Active sites require a minimum of 2 metal centres with flexible bridging

where oxygen can be stored and activated. If one wishes to designate this dynamic defect formation and healing as "surface lattice oxygen" then lattice oxygen is relevant. There arises the problem of distinction as any normal catalyst also provides under-coordinated sites for activating and storing reactants. Thus, the traditional statements that selective oxidation catalysts must have lattice oxygen and follow kinetically always the Mars-van Krevelan hypothesis are to be considered with reservation.

- *Site isolation:* The structural defects in V_xO_y provide site isolation both geometrically and electronically. It is current practice but not essential to achieve this by addition of foreign atoms or promoters. In agreement with literature there seems good evidence that a dimer of vanadium with another metal (vanadium or other) is the core active site highlighting the importance of reversible bridging of M-O-M substructures for selective oxidation.
- *Design of good catalysts:* The core property is the structural dynamics without allowing irreversible transformation in close packed reduced forms. Open structures with a cluster-linker topology are most adequate as they allow for active sites isolated and stabilized by heteroatomic linkers into the matrix. The matrix may provide storage functions for active oxygen and electrons to buffer local deficits in chemically potential or preserve the topology of the active structure in temporal episodes of lacking partial pressure of reactants.
- *Phases:* Neither well-developed and ordered phase of known binary oxides nor fully disordered or amorphous matrices are suitable to provide structural dynamics. Supramolecular units are strongly hydrated and provide extensive solid acid functions leading to sometimes unwanted selectivity in C-C bond breaking. The successful system is a nanostructured extended solid.
- *Supports:* The nanostructure needs support to provide stability under the harsh reaction conditions. This can be done by alumina silica or more functional supports like ceria or titania. Most suitable seems however self supporting. The active oxide is very well self-supported on the bulk of the matrix or precursor structure. This minimizes the adverse effect of unwanted reactivity of the support surface (water mediated C-C bond cracking) and optimizes the interaction of the active material with the support through homonuclear M-O-M bonds. For the characterisation of the active material, the problem of detection of an adlayer of similar composition but different structure arises.

Acknowledgements

The authors acknowledge financial support by SFB 546 of the Deutsche Forschungsgemeinschaft (DFG). W. Ranke is acknowledged for providing the schematic drawing of the reactor.

References

[1] E.A. Mamedov, V. Cortés Corberán, Appl. Catal. A 127 (1995) 1.
[2] E. Hums, Catal. Today 42 (1998) 25.
[3] B.M. Weckhuysen, D.E. Keller, Catal. Today 78 (2003) 25.
[4] G. Centi (Ed.), Vanadyl Pyrophosphate Catalyst, Catalysis Today, vol. 16, Part1, Elsevier, Amsterdam, 1993.
[5] R.L. Bergmann, N.W. Frisch, US Patent 3,393,368 (1968) assigned to Princton Chemical Research.
[6] T.R. Felthouse, J.C. Burnett, S.F. Mitchell, M.J. Mummy, Kirk-Othmer Encyclopedia of Chemical Technology, Wiley, New York, 1995.
[7] V.V. Guliants, J.B. Benzinger, N.Y. Sundaresan, I.E. Wachs, Catal. Lett. 32 (1995) 379.
[8] G.J. Hutchings, J.A. Lopez-Sanchez, J.K. Bartley, J.M. Webster, A. Burrows, C.J. Kiely, A.F. Carley, C.Rhodes, M. Hävecker, A. Knop-Gericke, R.W. Meyer, R.Schlögl, J.C. Volta, M. Poliakoff, J. Catal. 208 (2002) 197.
[9] I.E. Wachs, J.-M. Jehng, G. Deo, B.M. Weckhuysen, V.V. Guiliants, J.B. Benzinger, Catal. Today 32 (1996) 47.
[10] E. Kleimenov, H. Bluhm, M. Hävecker, A. Knop-Gericke, A. Pestryakov, D. Teschner, J. A. Lopez-Sanchez, J. K. Bartley, G.J. Hutchings, R. Schlögl, Surface Science 575 (2005) 181.
[11] M. Hävecker, R.W. Mayer, A. Knop-Gericke, H. Bluhm, E. Kleimenov, A. Liskowski, D.S. Su, R. Follath, F.G. Requejo, D.F. Ogletree, M. Salmeron, J.A. Lopez-Sanchez, J.K. Bartley, G.J. Hutchings, R. Schlögl, J. Phys. Chem. B 107 (2003) 4587.
[12] I.E. Wachs, B.M. Weckhuysen, Appl. Catal. A 157 (1997) 67.
[13] I.E. Wachs, J.M. Jehng, G. Deo, B.M. Weckhuysen, V.V. Guliants, J.B. Benziger, and S. Sundaresan, J. Catal. 170 (1997) 75.
[14] N.Pinna, M. Antonietti, M. Niederberger, Colloids Surf. A 250 (2004) 211.
[15] M. Niederberger, N. Pinna, J. Polleux, M. Antonietti, Angew. Chem. Int. Ed. 43 (2004) 2270.
[16] M. Niederberger, G. Garnweitner, N. Pinna, M. Antonietti, J. Am. Chem. Soc. 126 (2004) 9120.
[17] N. Pinna, G. Neri, M. Antonietti, M. Niederberger, Angew. Chem. Int. Ed. 43 (2004) 4345.
[18] N. Pinna, G. Garnweitner, M. Antonietti, M. Niederberger, Adv. Mater. 16 (2004) 2196.
[19] J. Le Bars, J.C. Vedrine, A. Auroux, B. Pommier, G.M. Pajonk, J. Phys. Chem. 96 (1992) 2217.
[20] L. Owens, H.H. Kung, J. Catal. 144 (1993) 202.
[21] A.-C. Dupuis, M. Abu Haija, B. Richter, H. Kuhlenbeck, H.-J. Freund, Surf. Sci. 539 (2003) 99.
[22] N. Magg, J.B. Giorgi, A. Hammoudeh, Th. Schroeder, M. Bäumer, H.-J. Freund, J. Phys. Chem. B 107 (2003) 9003.
[23] N. Magg, J.B. Giorgi, M.M. Frank, B. Immaraporn, Th. Schroeder, M. Bäumer, H.-J. Freund, J. Am. Chem. Soc. 126 (2004) 3616.
[24] C. Kuhrs, M. Swoboda, W. Weiss, Topics in Catal. 15 (2001) 13.
[25] W. Lindinger, A. Hansel, A. Jordan, Int. J. Mass Spec. 173 (1998) 191.

[26] W. Lindinger, A. Hansel, Plasma Sources Sci. Technol. 6 (1997) 111.
[27] K. Noack, H. Zbinden, R. Schlögl, Catal. Lett. 4 (1990) 145.
[28] G. Centi, F. Trifiro, J.R. Ebner, V.M. Franchetti, Chem. Rev. 88 (1988) 58.
[29] R.D. Leapman and L.A. Grunes, Phys. Rev. Lett. 45 (1980) 397.
[30] J. Fink, Th. Müller-Heinzerling, B. Scheerer, W. Speier, F.U. Hillebrecht, J.C. Fuggle, J. Zaanen, and G.A. Sawatzky, Phys. Rev. B 32 (1985) 4899.
[31] D.S. Su, M. Wieske, E. Beckmann, A. Blume, G. Mestl, and R. Schlögl, Catal. Lett. 75 (2001) 81.
[32] J.T. Gleaves and G. Centi, Catal. Today 16 (1993) 69.
[33] M. Ruitenbeek, R.A. Overbeek, A.J. van Dillen, D.C. Koningsberger, and J.W. Geus, Recl. Trav. Chim. Pays-Bas 115 (1996) 519.
[34] I.E. Wachs, Catal. Today 27 (1996) 437.
[35] B. Chen and E.J. Munson, J. Am. Chem. Soc. 124 (2002) 1638.